LETTER

Growth zoning and strain patterns inside diamond crystals as revealed by Raman maps

LUTZ NASDALA,[1,]* WOLFGANG HOFMEISTER,[1] JEFFREY W. HARRIS,[2] AND JÜRGEN GLINNEMANN[3]

[1]Institut für Geowissenschaften—Mineralogie, Johannes Gutenberg-Universität, D-55099 Mainz, Germany
[2]Division of Earth Sciences, University of Glasgow, Glasgow G12 8QQ, United Kingdom
[3]Institut für Mineralogie, Johann Wolfgang Goethe-Universität, D-60054 Frankfurt/Main, Germany

ABSTRACT

The Raman mapping technique provides a non-destructive means of studying internal growth textures and other micro-structural heterogeneity inside diamond single-crystals. Raman maps showing distribution patterns of the bandwidth (FWHM) of the main first-order lattice vibration of diamond (*LO=TO* phonon at ~1332 cm^{-1}) along two-dimensional planes inside diamond crystals may reveal the internal growth zoning of these crystals. The observed zoning is affected, and in some cases even obscured in micro-areas adjacent to inclusions, by patterns of heterogeneous strain in the diamond. We present Raman maps obtained from diamond crystals containing large, single-crystal graphite inclusions, from the Panda kimberlite, Ekati Diamond Mine, Canada. The diamond growth texture was always found to start from the graphite inclusion. This result implies that graphite must have been the primary phase and was overgrown by diamond, whereas syngenetic growth of diamond and graphite was unlikely.

INTRODUCTION

Graphite (α-C) is commonly found included in diamond (β-C) crystals (e.g., Harris and Gurney 1979), however, such inclusions are mostly thin, xenomorphic flakes or lamellae. In contrast, the occurrence of euhedral graphite crystals inside diamond crystals seems to be extremely rare, and their formation has long been debated (e.g., Bulanova et al. 1979). In a recent study, Glinnemann et al. (2003) described a suite of octahedral diamond crystals from the Panda kimberlite (Slave Craton), part of the Ekati Mine, N.W. Territories, Canada, each of them having included a well-shaped graphite single-crystal of hexagonal-platy habit, up to 300 μm in size. Glinnemann et al. (2003) found from graphite lattice parameters determined by X-ray diffraction that remnant pressures of up to 2.6 GPa act on the inclusions. Nasdala et al. (2003) determined corresponding remnant pressures of diamond micro-areas adjacent to the graphite inclusions, and they found the presence of disordered graphitic (i.e., sp^2) carbon at disc-shaped cracks that surround the well-ordered graphite single-crystals. Further detailed in situ analysis of these graphite inclusions and their surrounding diamond, including synchroton micro-analysis, is currently in process.

The formation of diamond crystals with an included euhedral graphite crystal has not been understood thus far. In particular, it has been discussed controversially whether such single-crystal graphite inclusions are proto- or syngenetic in nature. Valuable information contributing to genetic questions could be obtained through the study of growth zoning in the diamond host close to the diamond-inclusion boundary. The growth zoning of diamond is mostly observed applying the CL (cathodoluminescence) imaging technique (e.g., Smirnova et al. 1999; Win et al. 2001;

Davies et al. 2003). Due to the extremely low penetration depth of an electron beam, however, CL imaging is rather a surface technique and requires, in most cases, that the internal growth texture of diamond be exposed to a polished surface. In our case, this in turn would result in the irreversible pressure relaxation of the diamond+inclusion couple, which is why detailed CL studies cannot be done until all in situ studies will be completed.

As an alternative, confocal light spectroscopy techniques [i.e., Raman and PL (photoluminescence) spectroscopy] have the potential to reveal the growth zoning of diamond crystals in situ. Photoluminescence induced with ultraviolet light has been applied successfully to study the bulk growth zoning in unprepared diamond specimens (e.g., Bulanova 1995); however, attempts to produce depth-resolved images based on confocal PL measurements have, to the best of our knowledge, not been undertaken thus far. In this paper, we will demonstrate with the example of the above-described Panda diamond crystals with included graphite single-crystals that growth textures along planes inside diamond crystals are revealed using the Raman mapping technique. We discuss briefly the relevance of such information in the context of the genetic relationships between graphite inclusion and diamond host.

EXPERIMENTAL METHODS

Raman measurements were done in the confocal mode by means of a Jobin Yvon (Horiba group) LabRam HR spectrometer. The system was equipped with an Olympus BX41 optical microscope and an Si-based CCD (charge-coupled device) detector. A 100× long working distance objective (lwd ~4.6 mm, numerical aperture 0.75) was used. Spectra were excited with the 632.8 nm emission of a He-Ne laser. The laser power was ~3 mW, which is well below the threshold for any spectral changes, or local sample destruction, which hypothetically could be induced by local temperature increase due to heavy light absorption. The scattered light was dispersed using a grating with 1800 grooves per mm, which resulted in a spectral resolution of 0.8 cm^{-1}. The wavenumber accuracy was 0.5 cm^{-1}, how-

* E-mail: nasdala@uni-mainz.de

745

ever, the internal wavenumber reproducibility within maps (i.e., under uniform experimental conditions) was assessed at ~0.1 cm^{-1}. Band fitting was done after linear background correction and assuming the *LO=TO* signal to have a symmetric Lorentzian-Gaussian band profile.

Mapping was done using a motorized, software-controlled x-y stage. A Raman spectrum was acquired at each sampling point, thus producing hyperspectral data sets consisting of 20 000–100 000 single Raman spectra. Color-coded images (i.e., plots of a selected spectral parameter vs. the x-y coordinates of the respective sampling point) were then produced after appropriate data reduction. The volume resolution of the finally generated "tomographic images" is mainly limited by the real volume resolution of single Raman measurements (even though it may be additionally affected by the step width between sampling points). The analyzed x-y planes were 700–1100 μm behind the diamond surface. The confocality and, with that, the real volume resolution of single measurements placed that far behind a sample surface must be considered poorer than in the case of a surface-focused measurement (e.g., Everall 2000; Baldwin and Batchelder 2001). We estimate the lateral resolution of Raman maps presented in this study at 3–6 μm, and the depth resolution was probably as low as several tens of μm.

RESULTS AND DISCUSSION

Examples for typical Raman spectra as obtained in the present study are shown in Figure 1. The first-order Raman spectrum of diamond consists of only one (triply degenerate) band. This mode is usually referred to as *LO=TO* mode, because the optical vibrations of diamond are degenerate due to the high point-group symmetry of the crystal structure, and longitudinal-transverse splitting does not occur. At ambient pressure-temperature conditions, the *LO=TO* band has a nearly symmetric shape and is characterized by a Raman shift of ~1332 cm^{-1} and a narrow FWHM (full band width at half band maximum intensity) of ~1.6 cm^{-1} (e.g., Solin and Ramdas 1970). With increasing pressure and compressive strain, the *LO=TO* phonon shifts toward higher wavenumbers (e.g., Mitra et al. 1969; Grimsditch et al. 1978; Hanfland et al. 1985; Tardieu et al. 1990), which is accompanied by a FWHM increase (Fig. 1) and often also notable band asymmetry (e.g., Sharma et al. 1985). Based on calibrations of the *LO=TO* frequency increase in dependence of the crystallographic orientation, the Raman technique provides a means of quantifying internal pressure and strain inside diamond crystals, and it was shown by Nasdala et al. (2003) that high-pressure inclusions in diamond may be surrounded by haloes of remnant increased pressure and strain several hundred μm across.

The single-crystal graphite inclusions described in the present study must have experienced preferential expansion along their crystallographic **c**-axis (cf., Zhao and Spain 1989) during uplift and external pressure release. As a consequence, complete pressure relaxation was hindered in the neighboring diamond. Diamond areas adjacent to the graphite (001) faces in sample PAG12 yielded *LO=TO* Raman shifts of up to 1336.7 cm^{-1}. Assuming these micro-areas are mainly affected by uniaxial stress, rather than hydrostatic stress, and based on the respective calibration for uniaxial stress along [111] by Grimsditch et al. (1978), the observed maximum upshift of +4.9 cm^{-1} with respect to the bulk diamond host (*LO=TO* ~1331.8 cm^{-1}; see Figs. 1 and 2f) indicates a remnant pressure of ~2.2 GPa. This estimate is in good agreement with a remnant pressure of 2.1 GPa calculated from graphite lattice parameters (Glinnemann et al. 2003). By contrast, measured upshifts of the graphite G band (observed Raman shifts scattering in the range 1587–1599 cm^{-1}) would correspond to pressures in the range 1.7–4.7 GPa (cf., Liu et al. 1990). These apparently too-high pressure values, and their
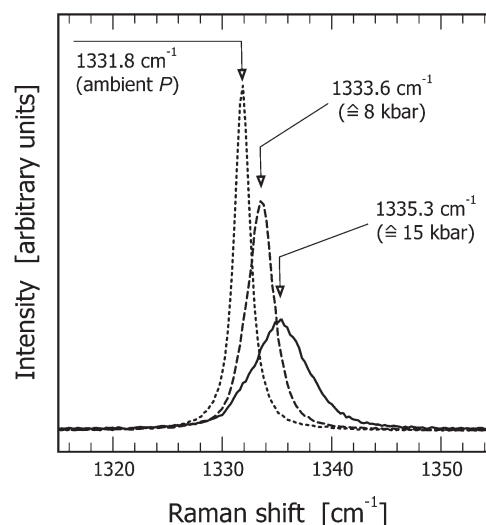

FIGURE 1. Raman spectra of three micro-areas at the surface and inside diamond specimen PAG12. Increased remnant pressure (compressive strain) is indicated by the increased Raman shift of the diamond *LO=TO* phonon. Remnant pressures were assigned based on the calibrations of Grimsditch et al. (1978) and Sharma et al. (1985).

large scatter, may indicate difficulties with using graphite for the determination of remnant pressures.

Outside those pressure-strain haloes surrounding graphite inclusions in Panda diamond samples, uniform diamond *LO=TO* Raman shifts of ~1332 cm^{-1} were obtained, without any indication for additional internal diamond heterogeneity (i.e., structural differences among growth zones do not notably affect the Raman shift of the *LO=TO* mode). We found that, by contrast, color-coded plots of the FWHM of the *LO=TO* mode reveal very well the internal growth texture of diamond crystals (see the planar patterns in Figs. 2b and 2d). Growth zones may differ in terms of their chemical composition (e.g., trace elements) and structural defects (e.g., point defect density), and we interpret such various degrees of lattice imperfections to be reflected by varying phonon lifetimes (i.e., FWHMs; see, for example, Surovtsev et al. 1999). Note that measured FWHM variations among growth zones are rather slight (less than 0.5 cm^{-1}), which seems to correspond well to the expected very minor structural differences among growth zones in diamond specimens that appear visually unzoned to the unaided eye.

We found in all cases that the diamond growth texture is controlled by {111}; two examples are given in Figure 2. In Raman maps parallel to a diamond (111) plane (i.e., view along a threefold axis; Fig. 2b), there are three growth-plane orientations with an angle of approximately 120° (Fig. 2b). Raman maps parallel to a diamond (110) plane (i.e., view along a twofold axis) show the expected two major orientations of octahedral growth planes with inter-plane angles of approximately 70.5° and 109.5°, respectively (Fig. 2d). Note that the somewhat "blurred" appearance of growth zones in Figure 2b is due to the limited depth resolution and the fact that growth planes are inclined with respect to the line of vision, whereas the growth texture in Figure 2d (view along growth planes) is less affected by the depth
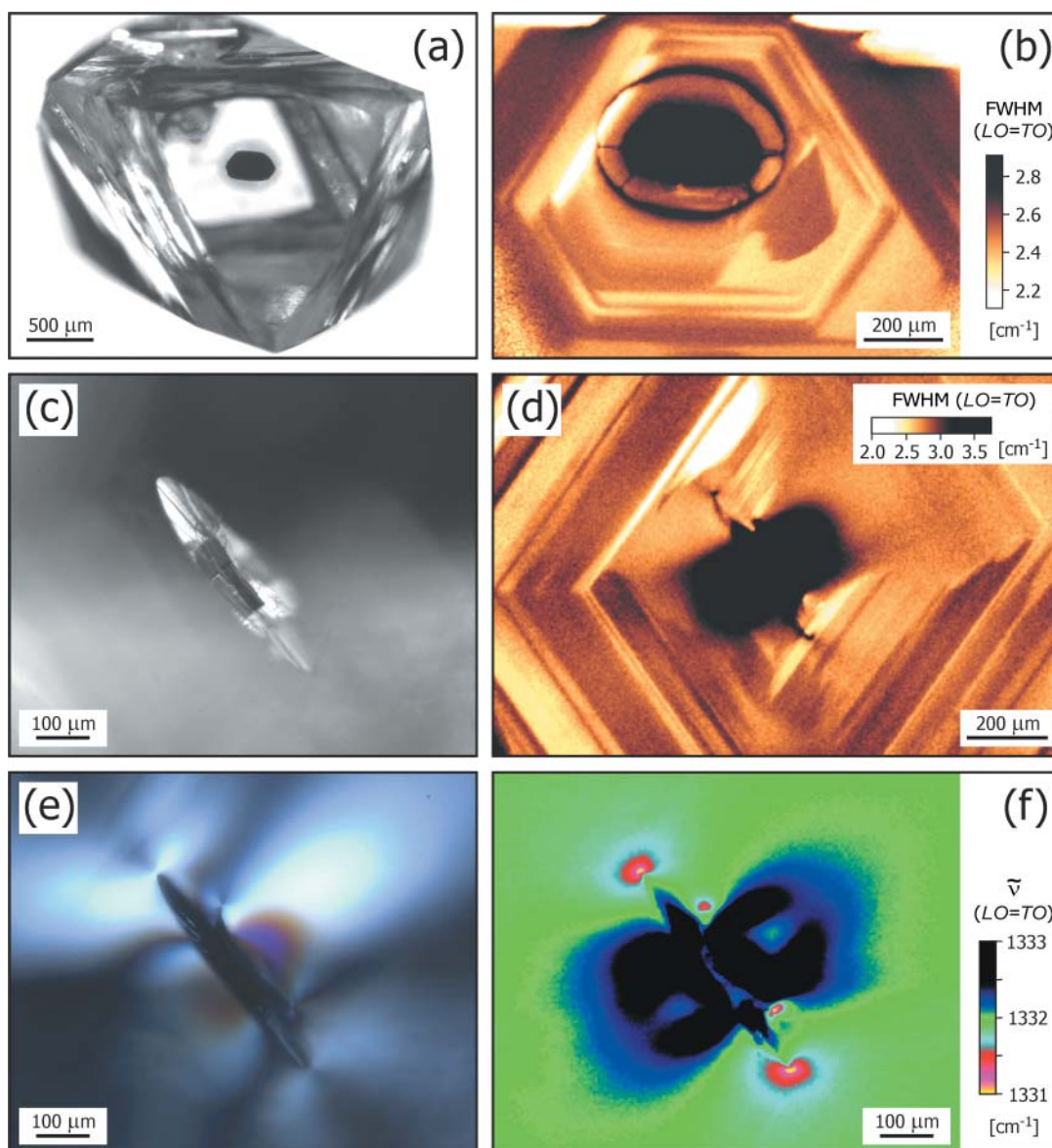
FIGURE 2. Photomicrographs and Raman maps of two diamond crystals from the Panda kimberlite. Sample PAG03: (**a**) View along [111]. The graphite inclusion is located more than 1 mm below a diamond (111) face. A small disc-like, ellipsoidal fracture in the diamond surrounding the graphite is indicated by light grayish color. (**b**) Raman map based on the FWHM of the diamond $LO=TO$ band. The octahedral growth zoning is overprinted by a pattern (black) of intense strain in the diamond host, close to the graphite crystal and right outside the ellipsoidal fracture. Sample PAG12: (**c**) Photomicrograph of the graphite inclusion. View along diamond [110] [which is reasonably close to along graphite (001)]. (**d**) Raman map (sampling depth ~700 μm behind the diamond surface), revealing the diamond's growth texture and internal strain pattern. (**e**) Photomicrograph, cross-polarized light. Note the brownish to violet-blue interference colors of the diamond close to the graphite (001) faces. (**f**) Raman map of the same area as shown in Figures c and e, based on the frequency of the $LO=TO$ phonon. Areas without notable strain are visualized green (measured Raman shift ~1332 cm^{-1}). Micro-areas affected by compressive strain (i.e., remnant internal pressure) are blue-black, and those affected by strong dilative strain (close to the ends of fractures) are red-yellow.

resolution and, therefore, it appears better resolved. The most important observation, however, is that in all cases, the origin of the growth texture is the location of the graphite inclusion, with the single-crystal graphite being virtually surrounded evenly by diamond growth zones.

The patterns of internal diamond growth zoning observed in the present study [revealed by minor differences among rather

narrow FWHM ($LO=TO$) values determined from different growth zones] are always overlaid by another pattern of micro-areas yielding much broader FWHMs (cf., central black areas in Figs. 2b and 2d). The latter match widely with the extension of micro-areas in which increased or decreased frequencies of the $LO=TO$ mode were observed and, therefore, they are interpreted as patterns of internal strain. It can be seen clearly in Figure 2b

that diamond PAG03 shows notable strain: (1) in micro-areas immediately neighbored with the graphite inclusion, and (2) outside of the rim of the ellipsoidal, disc-shaped crack surrounding the graphite inclusion. The strain pattern in sample PAG12 (Fig. 2d) consists of the same two principal components. To support this interpretation, we also present the corresponding map based on the Raman shift of the $LO=TO$ mode in Figure 2f. Note that the latter is equal in scale to the microphotograph in Figure 2c, showing that the **c**-axis of the tabular graphite crystal is oriented roughly SW-NE. Correspondingly, remnant enhanced pressure and compressive strain is particularly observed in diamond areas "left below" and "right above" the graphite inclusion. Particularly intense strain in these areas is also indicated by 1st order yellow-brownish up to 2nd order violet-blue interference colors in these areas (Fig. 2e; cf., Varshavskiy 1968; see also discussion by Zhang 1998). Dilative strain of lesser intensity occurs directly outside the ends of the two disc-shaped cracks in the diamond that surround the graphite inclusion (cf., lowered $LO=TO$ Raman shifts indicated by red to yellow color in Fig. 2f; downshift up to -0.8 cm^{-1}).

We have shown that Raman maps based on the FWHM of the diamond $LO=TO$ mode contribute to the in situ study of the growth zoning of diamond crystals. Our observations suggest, however, that this Raman parameter is sensitively affected by strain and, therefore, growth textures as revealed by comparably moderate FWHM variations may be biased, and in extreme cases even obscured, in micro-areas affected by intense strain. In the case of the Panda diamond samples discussed in this paper, the observed growth textures (along with the observation of crystallographic relationships between graphite and diamond host; cf. Glinnemann et al. 2003) indicate that bulk diamond has overgrown topotactically pre-existing graphite crystals, which characterizes the graphite inclusions as protogenetic in nature. Thus, syngenetic formation of both graphite and diamond appears most unlikely. One possible mechanism for diamond nucleation at the surface of pre-existing graphite crystals has been proposed by Lambrecht et al. (1993).

The Panda diamond samples seem to have grown relatively close to the graphite-diamond equilibrium boundary (cf., Kennedy and Kennedy 1976; Bundy et al. 1996). This is suggested by the observation that some of the graphite inclusions are extremely well preserved (see again Fig. 2c) and do not show any indication for the beginning of decomposition or transformation, which could be expected for a graphite crystal far in the diamond stability field. On the other hand, it is well known that, depending on the temperature and stress-strain regime, pressures of direct graphite-to-diamond transformation may be significantly higher than equilibrium pressures (e.g., Leshchuk et al. 2002). It seems worthwhile to subject future investigations, including transmission electron microscopy, to the sub-micrometer scale study of the graphite-diamond intergrowth at inclusion-host boundaries.

REFERENCES CITED

Baldwin, K.J. and Batchelder, D.N. (2001) Confocal Raman microspectroscopy through a planar interface. Applied Spectroscopy, 55, 517–524.

Beran, A. and Libowitzky, E., Eds. (2004) Spectroscopic methods in Mineralogy, 662 p. European Mineralogical Union Notes in Mineralogy, 6, Eötvös University Press, Budapest.

Bulanova, G.P. (1995) The formation of diamond. Journal of Geochemical Exploration, 53, 1–23.

Bulanova, G.P., Varshavskiy, A.V., Leskova, N.V., and Nikishova, N.V. (1979) On "central" inclusions in natural diamonds. Doklady Akademii Nauk SSSR, 244, 704–706 (in Russian).

Bundy, F.P., Bassett, W.A., Weathers, M.S., Hemley, R.J., Mao, H.U., and Goncharov, A.F. (1996) The pressure-temperature phase and transformation diagram for carbon; updated through 1994. Carbon, 34, 141–153.

Davies, R.M., Griffin, W.L., O'Reilly, S.Y., and Andrew, A.S. (2003) Unusual mineral inclusions and carbon isotopes of alluvial diamonds from Bingara, eastern Australia. Lithos, 69, 51–66.

Everall, N.J. (2000) Modeling and measuring the effect of refraction on the depth resolution of confocal Raman microscopy. Applied Spectroscopy, 54, 773–782.

Glinnemann, J., Kusaka, K., and Harris, J.W. (2003) Oriented graphite single-crystal inclusions in diamond. Zeitschrift für Kristallographie, 218, 733–739.

Grimsditch, M.H., Anastassakis, E., and Cardona, M. (1978) Effect of uniaxial stress on the zone-center optical phonon of diamond. Physical Review B, 18, 901–904.

Hanfland, M., Syassen, K., Fahy, S., Louie, S.G., and Cohen, M.L. (1985) Pressure dependence of the first-order Raman mode in diamond. Physical Review B, 31, 6896–6899.

Harris, J.W. and Gurney, J.J. (1979) Inclusions in diamond. In J.E. Field, Ed., The properties of diamond, p. 555–591. Academic Press, London.

Kennedy, C.S. and Kennedy, G.C. (1976) The equilibrium boundary between graphite and diamond. Journal of Geophysical Research, 81, 2467–2470.

Lambrecht, W.R.L., Lee, C.H., Segall, B., Angus, J.C., Li, Z., and Sunkara, M. (1993) Diamond nucleation by hydrogenation of the edges of graphitic precursors. Nature, 364, 607–610.

Leshchuk, A.A., Novikov, N.V., and Levitas, V.I. (2002) Thermomechanical model of the graphite → diamond phase transformation. Journal of Superhard Materials, 24, 44–52.

Liu, Z., Wang, L., Zhao, Y., Cui, Q., and Zou, G. (1990) High-pressure Raman studies of graphite and ferric chloride-graphite. Journal of Physics: Condensed Matter, 2, 8083–8088.

Mitra, S.S., Brafman, O., Daniels, W.B., and Crawford, R.K. (1969) Pressure-induced phonon frequency shifts measured by Raman scattering. Physical Review, 186, 942–944.

Nasdala, L., Brenker, F.E., Glinnemann, J., Hofmeister, W., Gasparik, T., Harris, J.W., Stachel, T., and Reese, I. (2003) Spectroscopic 2D-tomography: Residual pressure and strain around mineral inclusions in diamonds. European Journal of Mineralogy, 15, 931–935.

Sharma, S.K., Mao, H.K., Bell, P.M., and Xu, J.A. (1985) Measurement of stress in diamond anvils with micro-Raman spectroscopy. Journal of Raman Spectroscopy, 16, 350–352.

Smirnova, E.P., Zezin, R.B., Saparin, G.V., and Obyden, S.K. (1999) Color cathodoluminescence of natural diamond with a curvilinear zonality and orbicular core. Doklady Earth Sciences, 366, 522–525.

Solin, S.A. and Ramdas, A.K. (1970) Raman spectrum of diamond. Physical Review B, 1, 1687–1698.

Surovtsev, N.V., Kupriyanov, I.N., Malinovsky, V.K., Gusev, V.A., and Palyanov, Yu.N. (1999) Effect of nitrogen impurities on the Raman line width in diamonds. Journal of Physics: Condensed Matter, 11, 4767–4774.

Tardieu, A, Cansell, F., and Petitet, J.P. (1990) Pressure and temperature dependence of the first-order Raman mode of diamond. Journal of Applied Physics, 68, 3243–3245.

Varshavskiy, A.V. (1968) Anomalous birefringence and internal morphology of diamonds. 89 pp. Nauka, Moscow (in Russian).

Win, T.T., Davies, R.M., Griffin, W.L., Wathanakul, P., and French, D.H. (2001) Distribution and characteristics of diamonds from Myanmar. Journal of Asian Earth Sciences, 19, 563–577.

Zhang, Y.X. (1998) Mechanical and phase equilibria in inclusion-host systems. Earth and Planetary Science Letters, 157, 209–222.

Zhao, Y.X. and Spain, I.L. (1989) X-ray diffraction data for graphite to 20 GPa. Physical Review B, 40, 993–997.